Dalton Transactions

ROYAL SOCIETY OF CHEMISTRY

COMMUNICATION

View Article Online
View Journal | View Issue

Cite this: *Dalton Trans.*, 2021, **50**, 13227

Received 27th July 2021,
Accepted 2nd September 2021

DOI: 10.1039/d1dt02479e

rsc.li/dalton

A facile approach to prepare silica hybrid, spin-crossover water-soluble nanoparticles as potential candidates for thermally responsive MRI agents†

Patroula Gkolfi,[a] Dimitra Tsivaka,[b] Ioannis Tsougos,*[b] Katerina Vassiou,[c] Ondřej Malina, *[d] Michaela Polaskova,[d,e] Christina D. Polyzou,*[a] Christos T. Chasapis [f] and Vassilis Tangoulis *[a]

A reverse micelle method was used for the synthesis of water-soluble silica hybrid, spin-crossover (SCO) nanoparticles (NPs). MRI experiments provided temperature dependent *T*2 values, indicating their potential use as smart MRI agents, while lyophilization of NP dispersions in water yielded powders with a preserved but modified thermal hysteretic magnetic profile.

Spin-crossover (SCO) materials have been demonstrated as "newcomers" in the field of MRI as they tend to replace the classic Gadolinium-Based Contrast Agents (GBCAs) due to their association with nephrogenic systemic fibrosis (NSF).[1–4] Super-Paramagnetic Iron Oxide Nanoparticles (SPION)[5–9] and Paramagnetic CEST (ParaCEST) agents[10–13] are also classified as effective MRI contrast agents[14,15] displaying superior magnetic properties and biocompatibility.

SCO coordination polymers have been recently in the foreground since their magnetic properties in the solid state are attractive for their application as drug nanocarriers,[16–20] in cancer treatment[21,22] and as MRI contrast agents.[23,24] SCO iron(II) compounds undergo a spin state change between LS (S = 0) and HS (S = 2) that is temperature dependent. These properties might be exploited in MRI for the detection of tumor cells in cancer as their usual temperature is higher than that of normal cells. However, when it comes to biological applications, these materials face strong limitations emerging mainly from their low solubility in biological media.[25] Tsukiashi *et al.*[26,27] reported for the first time water soluble spin-crossover (SCO) iron(II) nanoparticles (NPs) of the one-dimensional (1-D) coordination polymer $[Fe(Htrz)_{3-3X}(NH_2trz)_{3X}](BF_4)_2$ (Htrz = 1,2,4-1*H*-triazole, NH_2trz = 4-amino-1,2,4-triazole, and X = 0.1) coated with polyethylene glycol (PEG) for use as thermally-responsive MRI contrast agents. A very recent report by Cordani *et al.*[28] describes how the obstacle of low solubility in water is surpassed when the polymeric chain is shortened, ending up in trinuclear oligomers. The synthesized $[Fe_3(R\text{-}trz)_6]X_6$ trimers (R-trz = substituted triazole; X = counter anion) were used as synergistic adjuvants for pancreatic cancer.

In this context, we present the synthesis and spectroscopic characterization of silicon-modified doped NPs based on the already known 1-D SCO coordination polymer $[Fe^{II}(Htrz)_2(trz)](BF_4)$. In the literature, there have been reports[29–37] describing the magnetic properties of doped or/and silicon modified $[Fe^{II}(Htrz)_2(trz)](BF_4)$ NPs but without any success in the preservation of their stability in aqueous media. To the best of our knowledge, this is the very first example of doped aminated silica hybrid SCO CPs at the nanoscale in the literature displaying *stable aqueous colloidal dispersions*. The effective modification of their surfaces with SiO_2 is considered of great importance as the NPs create stable colloidal dispersions in water and thus are good candidates for potential application as MRI-contrast agents. The general formula of the synthesized NPs is $[Fe(Htrz)_2(trz)](BF_4)@SiO_2$ (**1**); for the ligand substituted NPs: $[Fe(Htrz)_{2.1}(trz)_{0.8}(NH_2trz)_{0.1}](BF_4)_{1.2}@SiO_2$ (**2**); for the ligand and metal substituted NPs : $[Fe_{0.9}Zn_{0.1}(Htrz)_{2.1}(trz)_{0.8}(NH_2trz)_{0.1}](BF_4)_{1.2}@SiO_2$ (**3**); for the ligand substituted NPs: $[Fe(Htrz)_2(trz)_{0.7}(NH_2trz)_{0.3}](BF_4)_{1.3}@SiO_2$ (**4**). All the NPs were synthesized at room temperature, using the reverse micelle technique (Fig. 1). To effectively shift the thermal hysteretic phenomenon, two different experimental procedures were fol-

[a]*Department of Chemistry, Laboratory of Inorganic Chemistry, University of Patras, 26504 Patras, Greece. E-mail: chpolyzou@upatras.gr, vtango@upatras.gr*
[b]*Department of Medical Physics, University Hospital of Larissa, University of Thessaly, Biopolis, GR-41110 Larissa, Greece. E-mail: tsougos@med.uth.gr*
[c]*Department of Radiology, University Hospital of Larissa, University of Thessaly, Biopolis, GR-41110 Larissa, Greece*
[d]*Regional Centre of Advanced Technologies and Materials, Czech Advanced Technology and Research Institute (CATRIN), Palacký University Olomouc, Czech Republic. E-mail: ondrej.malina@upol.cz*
[e]*Department of Experimental Physics, Faculty of Science, Palacký University Olomouc, 17. Listopadu 1192/12, 771 46 Olomouc, Czech Republic*
[f]*NMR Facility, Instrumental Analysis Laboratory, School of Natural Sciences, University of Patras, 26504 Patras, Greece*

†Electronic supplementary information (ESI) available: Synthetic details, UV/vis spectroscopy, P-XRD patterns, Differential Scanning Calorimetry (DSC), SEM/TEM microscopy, and additional figures. and tables. See DOI: 10.1039/d1dt02479e

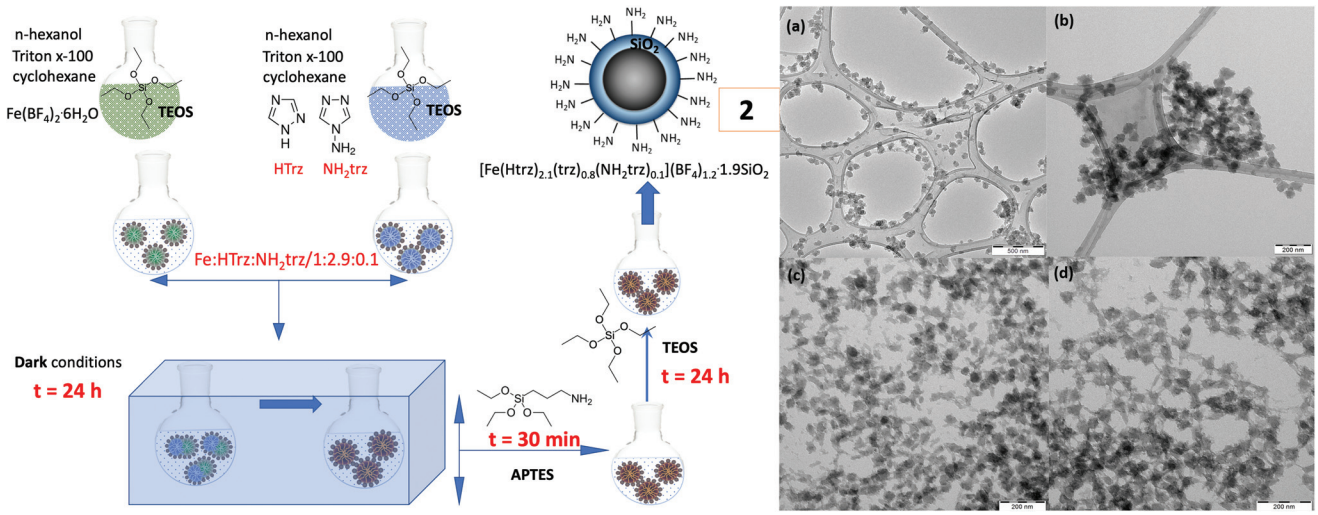

Fig. 1 (left) Synthetic strategy for the preparation of NPs **2**. (right) TEM images of NPs **1** (a), **2** (b), **3** (c) and **4** (d).

lowed: (a) the ligand substituted addition of the bulkier dopant NH_2trz ligand leading to a strong destabilization of the crystal lattice and (b) the metal and ligand co-substituted experimental protocol using as dopants both the Zn^{II} metal ion and the NH_2trz ligand, which is presented for the first time. The nature of the surfactant medium and the ratio of concentrations [Fe]/[HTrz], [Fe/Zn]/[HTrz/NH_2Trz] and [Fe]/[HTrz/NH_2Trz] were chosen carefully to accommodate two important prerequisites: (i) sphere-like monodisperse nanoparticles with sizes smaller than 40 nm and (ii) gradual SCO magnetic behavior in the temperature range of 280–320 K. Two water-in-oil (w/o) microemulsions were mixed with the organic phase consisting of certain amounts of surfactant (Triton X-100) and co-surfactants (*n*-hexanol and cyclohexane). The latter reagents also play the role of organic solvents. The first step of hydrolysis/condensation of TEOS (tetraethyl orthosilicate) is initiated with the addition of 100 μL of TEOS in the aqueous phase consisting of the respective metal salts and ligands each dissolved in 0.5 mL of deionized H_2O (Fig. 1). The second step of hydrolysis/condensation of APTES (3-aminopropyltriethoxy silane) or co-condensation of APTES/TEOS took place after mixing the two water-in-oil (w/o) microemulsions and leaving them under magnetic stirring for 24 hours (Fig. 1). In this step, either 100 μL of APTES were added to the final microemulsion to initiate a new condensation procedure (NPs **4**) or 100 μL of APTES/100 μL of TEOS were used for the co-condensation procedure (NPs **1**, **2**, and **3**). NPs **1** were prepared using the $Fe(BF_4)_2{\cdot}6H_2O$ and HTrz reagents in a 1 : 3 molar ratio in the aqueous phase. The polymer consists of two neutral Htrz ligands and one deprotonated trz ligand bridging the Fe^{II} metal ions and BF_4^- ions, compensating its total charge. Partial replacement—in a gradually increasing percentage—of $Fe(BF_4)_2{\cdot}6H_2O$ and the deprotonated trz ligand by $Zn(BF_4)_2{\cdot}6H_2O$ and the NH_2trz ligand, respectively, was performed. More explicitly, partial replacement of 10% of the deprotonated trz ligand by the NH_2trz derivative resulted in the formation of NPs **2**. The doped polymer was synthesized using the $Fe(BF_4)_2{\cdot}6H_2O$, HTrz and NH_2trz reagents in a 1 : 2.9 : 0.1 molar ratio. The doping reactions were continued in the next step by further replacement of 10% $Fe(BF_4)_2{\cdot}6H_2O$ by the Zn^{II} analogue. The molar ratio used for the preparation of NP**3**, after the addition of the $Fe(BF_4)_2{\cdot}6H_2O$, $Zn(BF_4)_2{\cdot}6H_2O$, HTrz and NH_2trz reagents was 0.9 : 0.1 : 2.9 : 0.1 (the Fe/Zn ratio is confirmed by EDS analysis; Fig. S1†). NPs **4** are considered as the most doped ones since the replacement of trz by NH_2trz reached the percentage of 30%. $Fe(BF_4)_2{\cdot}6H_2O$, HTrz and NH_2trz are the reagents used in a 1 : 2.7 : 0.3 molar ratio. The proposed compositions for the above-mentioned NPs, based on elemental analysis, took into consideration the mechanism presented by Piedrahita-Bello *et al.*[36] according to which the dopant NH_2trz ligand selectively replaces the deprotonated (trz) ligand instead of the neutral (HTrz) ligand, increasing the portion of BF_4^- accordingly.

The structure and detailed composition of the doped silicon-modified SCO NPs were determined by IR spectroscopy (Fig. S2†), X-ray powder diffraction (Fig. S3†) and elemental analysis (Table S1†). Particle dimensions and morphology were determined by transmission electron microscopy. Fig. S4† shows the size distribution for all the silicon-modified SCO NPs calculated based on the TEM images depicted in Fig. 2 and S5.† All the NPs are well-shaped adopting a sphere-like morphology accompanied by a very thin layer of SiO_2 of a few nanometers. According to the Gaussian distributions (Fig. S4†) and TEM images (Fig. 2 and S5†) as well, the NPs **1** present a larger mean diameter (~45 nm) than the rest of the NPs. Another interesting observation is that NPs **2** show an ultrasmall diameter (~10 nm) compared to NPs **3** and **4** with sizes close to 25 nm. Indeed, all the NPs present excellent homogeneity with few regions of minor aggregation due to the synthetic method chosen for their preparation.

It is remarkable to note that stable water colloidal dispersions of all NPs were prepared using ultrasonication (2 mg of

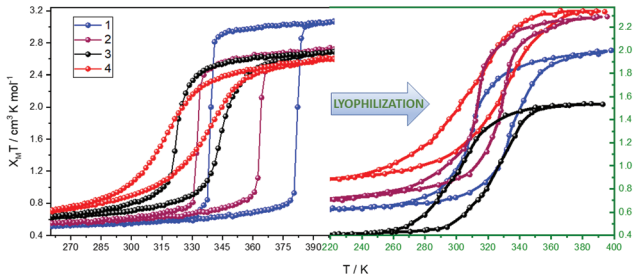

Fig. 2 Thermal dependence of the χ_MT product for NPs **1–4** with a rate of 1 K min^{-1} along with the lyophilized analogues.

NPs in 1 mL of H_2O). The color of all the dispersions changed from purple to colorless over a period of several minutes, revealing the evolution of the SCO phenomenon in water from the LS state to a fraction of the HS state of the Fe^{II} ion (a yellow color is expected for a fully recovered HS state of the Fe^{II} ion). Interestingly, all dispersions obtained their initial purple color when stored in a refrigerator (−20 °C), presenting excellent reversibility. From all our synthetic efforts, it is important to underline the synthetic conditions under which stable aqueous dispersions are obtained. It was observed that in the "non-doping" reaction (NPs **1**), where ascorbic acid was absent, the addition of a total of 300 μL of TEOS and 100 μL of APTES in a two-step hydrolysis/condensation procedure was necessary for the stabilization of the water dispersion. In the "doping" reactions (NPs **2**, **3**, and **4**), where ascorbic acid is included, the two-step hydrolysis/condensation procedure can be performed with lower volumes: 200 μL of TEOS and 100 μL of APTES (NPs **4**). When the above-mentioned volumes are further reduced, the behavior of the NPs in water changed dramatically. More explicitly, the color turned out to be yellowish without any possibility of the occurrence of the reversible process. In order to verify the reversibility of the SCO phenomenon in water, UV-vis measurements were carried out. Fig. S6† shows time-dependent UV-vis absorption spectra for NPs **1–4**: (a) when the samples are dispersed for the first time in H_2O and (b) during the thawing procedure (−20 °C – RT). In both cases, the absorption band around 280 nm—corresponding to an MLCT transition—showed a drastic reduction of its intensity as the samples switched from the LS to HS state of Fe^{II} accompanied by a color change in the dispersion from purple to colorless (Fig. S7 and S8†). The time duration of the SCO phenomenon calculated from the UV-vis experiments is presented in Table S3.†

DLS measurements of the aqueous dispersion of NPs (Fig. S9†) revealed a certain tendency to aggregate and their size increases to values close to 100 nm for NPs **1** and 50 nm for NPs **2**. In the case of NPs **3** and **4**, two distinctive size distributions are visible close to 20–30 nm and 200–300 nm. The estimated mean ζ-potential for all NPs has positive values greater than 30.0 mV (Fig. S10 and Table S4†), indicating the effective functionalization of their surface with amine groups, as well as the excellent quality of the colloid in water. Lyophilization of the latter aqueous dispersions resulted in powders with similar structural characteristics determined by IR spectroscopy (Fig. S2†) and X-Ray powder diffraction (Fig. S3a†). This observation may lead to the proposal that the aminated silica shell provides an effective shield to the NP core and furthermore stabilizes aqueous colloidal dispersions. A Pawley refinement was considered for all the NPs and their lyophilized analogues, and it was found that the powder patterns were consistent with the same unit cell and space group (*Pnma*) proposed for the $[Fe^{II}(Htrz)_2(trz)](BF_4)$ system with small calculated differences (Fig. S3b, Table S2†).[38,39]

Temperature-dependent magnetic measurements were carried out on samples **1–4** as well as on their lyophilized analogues and are shown in Fig. 2. In each case, the second thermal cycle was taken into consideration as the first one is usually related to the dehydration of the sample. Based on the magnetic study, we can amplify the strong evidence—which is also supported by the literature[29–37]—that metal and ligand substitution (here referred to as "doping") shifts the hysteresis clearly toward room temperature. The higher doping percentage is clearly the reason for the considerable shift of the hysteresis towards lower temperatures (NPs **3** and **4**). We cannot also overlook the loss of hysteresis abruptness and narrowing of its width as the doping percentage is increased. Quite surprisingly, the lyophilized materials preserve the SCO hysteretic character, which is observed, to our knowledge, for the first time. A shift of the hysteresis and a further narrowing of its width have been observed only in the cases of lyophilized NPs **1** and **2**, while for all the cases there is a suppression in the saturated χ_MT values (Table S5†) possibly due to the size effects and/or the hydrated form of the freeze-drying lyophilized samples. The SCO behavior exhibited by all the NPs was also confirmed through DSC measurements (Fig. S11†) as the critical temperatures coincide with those extracted from the magnetic study.

MRI T2 relaxometry studies are performed for the aqueous dispersions of all the NPs (Fig. S12–S18†). According to the thermal dependence of r_2 relaxivity (Fig. 3), NPs **3** and **4** are promising candidates for potential use as thermally responsive T2 MRI contrast agents with r_2 values in the range of 2.5–3.0

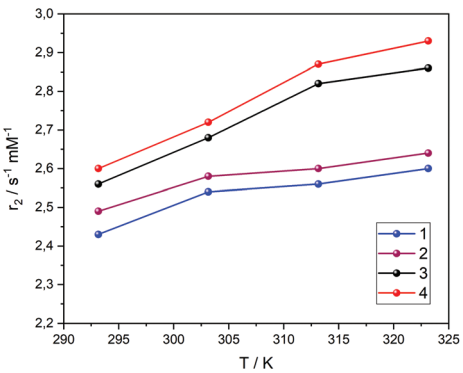

Fig. 3 Thermal dependence of the r_2 relaxivity of NPs **1–4**. The concentration used for the relaxometry studies was 3 mM.

s^{-1} mM^{-1} which is consistent with the values for commercially available MRI contrast agents[38] measured at 3 T in water. On the other hand, T1 relaxometry measurements (Fig. S19†) of NPs **3** and **4** also revealed temperature dependent $T1$ values that are significantly lower compared to those of GBCAs currently used for clinical diagnosis,[40] in accordance with the recent studies of PEG-modified SCO NPs.[27] The T1 and T2-w images of the phantom for NPs **3** and **4** at 20 °C and 50 °C at various inversion (TI) and echo (TE) times are shown in Fig. S18 and S19†, revealing their thermally responsive T2 character.

In conclusion, a two-step approach of the hydrolysis/condensation of TEOS/APTES is presented as an efficient synthetic path for the preparation of functional aminated silica hybrid SCO NPs of the general formula $[Fe_{1-Z}Zn_Z(Htrz)_{1+Y-X}(trz)_{2-Y}(NH_2trz)_X](BF_4)_Y@SiO_2$. Stable aqueous colloidal dispersions were prepared with a clear reversibility of the SCO phenomenon accompanied by a color change from colorless (HS state) to purple (LS state), while positive mean ζ-potential values greater than 30 mV were obtained for the SCO NPs, confirming an effective functionalization of their surface with amine groups as well as the excellent quality of the colloid in water. Lyophilization of the NP aqueous dispersions resulted in powders with similar structural characteristics, preserving the SCO hysteretic character. According to the MRI T2 relaxometry studies, the experimental doping protocols of (i) ligand substituted addition of the bulkier dopant NH_2trz ligand (NPs **4**) and (ii) metal and ligand co-substituted addition of Zn^{II}/NH_2trz (NPs **3**) provide thermally responsive T2 MRI contrast agents. Overall, our present communication describes an effective experimental tool for the preparation of water-soluble SCO NPs and we are confident that this information will encourage the scientific community working on the biological applications of these materials.

Conflicts of interest

There are no conflicts of interest.

Acknowledgements

This research was supported by a grant (80623) from the Research Committee of the University of Patras *via* the "C. CARATHEODORI" program. C. D. P. acknowledges the State Scholarships Foundation (IKY). This research is co-financed by Greece and the European Union (European Social Fund [ESF]) through the Operational Programme "Human Resources Development, Education and Lifelong Learning" in the context of the project "Reinforcement of Postdoctoral Researchers-2nd Cycle" (MIS-5033021), implemented by the State Scholarships Foundation (IKY). O.M. and M.P. would like to thank the following projects: the Research Infrastructure NanoEnviCz, supported by the Ministry of Education, Youth and Sports of the Czech Republic under Project No. LM2018124 and the ERDF/ESF project "Nano4Future" Development of Pre-applied Research in Nanotechnology and Biotechnology (no. CZ.02.1.01/0.0/0.0/17_048/0007323).

Notes and references

1 M. Edward, J. A. Quinn, S. Mukherjee, M. B. V. Jensen, A. G. Jardine, P. B. Mark and A. D. Burden, *J. Pathol.*, 2008, **5**, 584.
2 H. H. Abujudeh, *Radiology*, 2009, **1**, 81.
3 R. N. Hellman, *Semin. Nephrol.*, 2011, **3**, 310.
4 A. K. Abu-Alfa, *Adv. Chronic Kidney Dis.*, 2011, **3**, 188.
5 C. Tassa and S. Y. Shaw, *Acc. Chem. Res.*, 2011, **44**, 842.
6 J. Gao, H. Gu and B. Xu, *Acc. Chem. Res.*, 2009, **42**, 1097.
7 Y. X. J. Wang, S. M. Hussain and G. P. Krestin, *Eur. Radiol.*, 2001, **11**, 2319.
8 C. Corot, P. Robert, J. M. Idee and M. Port, *Adv. Drug Delivery Rev.*, 2006, **58**, 1471.
9 U. I. Tromsdorf, O. T. Bruns, S. C. Salmen, U. Beisiegel and H. Weller, *Nano Lett.*, 2009, **9**, 4434.
10 I. R. Jeon, J. G. Park, C. R. Haney and T. D. Harris, *Chem. Sci.*, 2014, **5**, 2461.
11 S. J. Dorazio, P. B. Tsitovich, K. E. Silters, J. A. Spernyak and J. R. Morrow, *J. Am. Chem. Soc.*, 2011, **133**, 14154.
12 S. J. Dorazio and J. R. Morrow, *Inorg. Chem.*, 2012, **51**, 7448.
13 S. J. Dorazio and J. R. Morrow, *Eur. J. Chem.*, 2012, 2006.
14 Z. Cai, C. Wu, L. Yang, D. Wang and H. Ai, *ACS Biomater. Sci. Eng.*, 2020, **6**, 2533.
15 J. Wahsner, E. M. Gale, A. Rodríguez-Rodríguez and P. Caravan, *Chem. Rev.*, 2019, **119**, 957.
16 Y. Hu, T. Lv, Y. Ma, J. Xu, Y. Zhang, Y. Hou, Z. Huang and Y. Ding, *Nano Lett.*, 2019, **19**, 2731.
17 M. Rezaei, A. Abbasi, R. Dinarvand, M. Jeddi-Tehrani and J. Janczak, *ACS Appl. Mater. Interfaces*, 2018, **10**, 17594.
18 C. He, C. Poon, C. Chan, S. D. Yamada and W. Lin, *J. Am. Chem. Soc.*, 2016, **138**, 6010.
19 I. Imaz, M. Rubio-Martínez, L. García-Fernández, F. García, D. Ruiz-Molina, J. Hernando, V. Puntes and D. Maspoch, *Chem. Commun.*, 2010, **46**, 4737.
20 X. Duan, C. Chan, W. Han, N. Guo, R. R. Weichselbaum and W. Lin, *Nat. Commun.*, 2019, **10**, 1899.
21 J. Liu, H. Wang, X. Yi, Y. Chao, Y. Geng, L. Xu, K. Yang and Z. Liu, *Adv. Funct. Mater.*, 2017, **27**, 1703832.
22 J. Liu, L. Tian, R. Zhang, Z. Dong, H. Wang and Z. Liu, *ACS Appl. Mater. Interfaces*, 2018, **10**, 43493.
23 S. Suárez-García, N. Arias-Ramos, C. Frias, A. P. Candiota, C. Arús, J. Lorenzo, D. Ruiz-Molina and F. Novio, *ACS Appl. Mater. Interfaces*, 2018, **10**, 38819.
24 Y. Chen, K. Ai, J. Liu, X. Ren, C. Jiang and L. Lu, *Biomaterials*, 2016, **77**, 198.
25 I. Bräunlich, A. Sánchez-Ferrer, M. Bauer, R. Schepper, P. Knüsel, J. Dshemuchadse, R. Mezzenga and W. Caseri, *Inorg. Chem.*, 2013, **53**, 3546.

26 A. Tsukiashi, K. S. Min, H. Terasawa, S. Yoshinaga, M. Takeda, R. Ohtani, M. Nakamura, L. F. Lndoy and S. Hayami, *Chem. Lett.*, 2018, **47**, 598.
27 A. Tsukiashi, K. S. Min, H. Kitayama, H. Terasawa, S. Yoshinaga, M. Takeda, L. F. Lindoy and S. Hayami, *Sci. Rep.*, 2018, **8**, 14911.
28 M. Cordani, E. Resines-Urien, A. Gamonal, P. Milán-Rois, L. Salmon, A. Bousseksou, J. S. Costa and A. Somoza, *Antioxidants*, 2021, **10**, 66.
29 E. Coronado, J. R. Galán-Mascarós, M. Monrabal-Capilla, J. García-Martínez and P. Pardo-Ibáñez, *Adv. Mater.*, 2007, **19**, 1359.
30 J. R. Galán-Mascarós, E. Coronado, A. Forment-Aliaga, M. Monrabal-Capilla, E. Pinilla-Cienfuegos and M. Ceolin, *Inorg. Chem.*, 2010, **49**, 5706.
31 S. Titos-Padilla, J. M. Herrera, X.-W. Chen, J. J. Delgado and E. Colacio, *Angew. Chem.*, 2011, **123**, 3348.
32 M. Giménez-Marqués, M. L. García-Sanz de Larrea and E. Coronado, *J. Mater. Chem. C*, 2015, **3**, 7946.
33 J. M. Herrera, S. Titos-Padilla, S. J. a. Pope, I. Berlanga, F. Zamora, J. J. Delgado, K. V. Kamenev, X. Wang, A. Prescimone, E. K. Brechin and E. Colacio, *J. Mater. Chem. C*, 2015, **3**, 7819.
34 I. Suleimanov, J. S. Costa, G. Molnár, L. Salmon and A. Bousseksou, *Chem. Commun.*, 2014, **50**, 13015.
35 S. Rat, M. Piedrahita-Bello, L. Salmon, G. Molnár, P. Demont and A. Bousseksou, *Adv. Mater.*, 2018, **8**, 1705275.
36 M. Piedrahita-Bello, K. Ridier, M. Mikolasek, G. Molnár, W. Nicolazzi, L. Salmon and A. Bousseksou, *Chem. Commun.*, 2019, **55**, 4769.
37 R. Torres-Cavanillas, L. Lima-Moya, F. D. Tichelaar, H. W. Zandbergen, M. Giménez-Marqués and E. Coronado, *Dalton Trans.*, 2019, **48**, 15465.
38 A. Grosjean, P. Négrier, P. Bordet, C. Etrillard, D. Mondieig, S. Pechev, E. Ledraud, J.-F. Létard and P. Guionneau, *Eur. J. Inorg. Chem.*, 2013, **5**, 796.
39 M. Palluel, L. E. Khoury, N. Daro, S. Buffière, M. Josse, M. Marchivie and G. Chastanet, *Inorg. Chem. Front.*, 2021, **8**, 3697.
40 M. Rohrer, H. Bauer, J. Mintorovitch, M. Requardt and H. J. Weinmann, *Invest. Radiol.*, 2005, **40**, 715.